Hybrid Perovskites

Deutsche Ausgabe: DOI: 10.1002/ange.201609529
Internationale Ausgabe: DOI: 10.1002/anie.201609529

Thin-Film Transformation of NH_4PbI_3 to $CH_3NH_3PbI_3$ Perovskite: A Methylamine-Induced Conversion–Healing Process

Yingxia Zong, Yuanyuan Zhou, Minggang Ju, Hector F. Garces, Amanda R. Krause, Fuxiang Ji, Guanglei Cui, Xiao Cheng Zeng, Nitin P. Padture,* and Shuping Pang**

Abstract: *Methylamine-induced thin-film transformation at room-temperature is discovered, where a porous, rough, polycrystalline NH_4PbI_3 non-perovskite thin film converts stepwise into a dense, ultrasmooth, textured $CH_3NH_3PbI_3$ perovskite thin film. Owing to the beneficial phase/structural development of the thin film, its photovoltaic properties undergo dramatic enhancement during this NH_4PbI_3-to-$CH_3NH_3PbI_3$ transformation process. The chemical origins of this transformation are studied at various length scales.*

Hybrid organic–inorganic perovskites (HOIPs) are a class of materials with the general formula ABX_3, where A is an organic cation, X is a halogen anion, and B is typically Pb^{2+}.[1] Their unique hybrid crystal structures have endowed these amazing HOIP materials interesting and unconventional properties, with great promise in a wide range of applications.[1,2] In particular, there has been a surge of interest in using HOIPs in solar cells.[2,3] Thus, enormous amount of effort is being devoted towards studying these materials, invoking new concepts in inorganic–organic hybrid chemistry.[4] Here, we report the discovery of a unique room-temperature thin-film transformation of NH_4PbI_3-to-$CH_3NH_3PbI_3$ induced by methylamine (CH_3NH_2) gas, and provide insights into its chemical origins.

The structure of ABX_3 is determined empirically by the Goldschmidt tolerance factor,[1] $t=(r_A+r_X)/\{\sqrt{2}(r_B+r_X)\}$, where r_A, r_B, and r_X are the radii of the A, B, and X, respectively. For NH_4PbI_3, t is 0.76.[5] In this context, at ambient temperature, instead of a stable 3D perovskite structure, NH_4PbI_3 usually exhibits a 1D non-perovskite structure (orthorhombic, space group *Pnma*).[6] This reduced structural dimensionality results in the relaxation of the band gap and, thus, NH_4PbI_3 appears yellow with a large indirect band gap >2 eV, as revealed by the Tauc plot (Figure S1 in the Supporting Information (SI)) and the band structure (Figure S2 in the SI) calculated using density functional theory (DFT). Furthermore, the 1D crystal structure of NH_4PbI_3 energetically favors the formation of high aspect ratio structures, instead of dense thin films, from simple "one-step" solution deposition. Such (opto)electronic and morphological characteristics suggest that the solution-grown NH_4PbI_3 is not a very useful material for single-junction solar cells.[7] Here we have discovered that a rough, porous, and polycrystalline NH_4PbI_3 non-perovskite thin film transforms into an ultrasmooth, dense, and textured $CH_3NH_3PbI_3$ ($MAPbI_3$) HOIP thin film by using a methylamine-induced conversion–healing process. As a result, the photovoltaic (PV) properties of the thin film undergo dramatic enhancement.

The transformation of NH_4PbI_3 was first observed in situ in bulk crystals using an optical microscope, as shown in Figure 1. The starting solution-grown NH_4PbI_3 crystal exhibits a rod-like morphology with a light-yellow color (Figure 1 A). Once methylamine (CH_3NH_2) gas is introduced, the crystal immediately turns black, with its rod-like morphology preserved (Figure 1 B). Subsequently, the rod surface begins to "melt", forming a clear, smooth liquid shell (Figure 1 C). After 1 min exposure to CH_3NH_2 gas, the solid rod completely transforms to a smooth liquid drop (Figure 1 D). When the CH_3NH_2 gas is removed, black specks nucleate within the liquid (Figure 1 E). Finally, a smooth black solid particle forms with a shape completely different from the original rod (Figure 1 F).

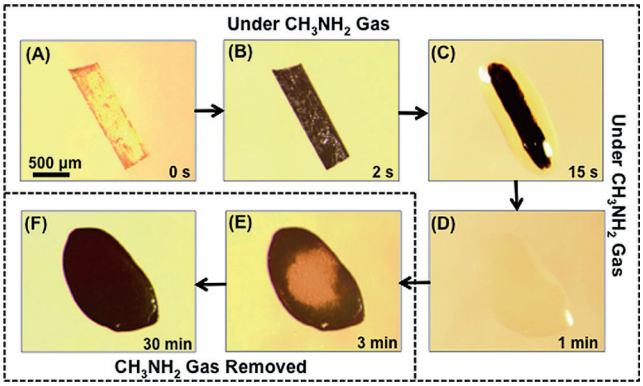

Figure 1. In situ optical microscope observation of the transformation of NH_4PbI_3 to $MAPbI_3$ induced by methylamine gas.

[*] Y. Zong, F. Ji, Dr. G. Cui, Dr. S. Pang
Qingdao Institute of Bioenergy and Bioprocess Technology
Chinese Academy of Sciences
Qingdao 266101 (P.R. China)
E-mail: pangsp@qibebt.ac.cn
Y. Zong, Dr. Y. Zhou, Dr. H. F. Garces, Dr. A. R. Krause, Prof. N. P. Padture
School of Engineering, Brown University
Providence, RI 02912 (USA)
E-mail: yuanyuan_zhou@brown.edu
nitin_padture@brown.edu
Dr. M. Ju, Prof. X. C. Zeng
Department of Chemistry, University of Nebraska
Lincoln, NE 68588 (USA)

Supporting information for this article can be found under: http://dx.doi.org/10.1002/anie.201609529.

Table 1: Description of the four stages of the thin-film transformation.

Stage	Description	Appearance
I	Starting NH_4PbI_3 thin film	yellow, opaque
II	Under CH_3NH_2 gas after 1 s	brown, opaque
III	Under CH_3NH_2 gas after 2 s	colorless, shiny
IV	2 s after removal of CH_3NH_2 gas	brown, shiny

In the case of NH_4PbI_3 thin films, such transformation behavior occurs very rapidly (within seconds), as expected, considering the nanoscale morphology of the thin films. Here, a starting NH_4PbI_3 thin film is processed simply by spin-coating a NH_4PbI_3 solution in dimethylformamide (DMF). As soon as the light-yellow color NH_4PbI_3 thin film (Figure 2A, Stage I) is exposed to CH_3NH_2 gas, it darkens within one second (Figure 2B, Stage II), and it becomes bleached after another second (Figure 2C, Stage III). The thin film is then removed from the CH_3NH_2 gas to the ambient, and a brown shiny thin film readily appears (Figure 2D Stage IV). Figures 2E–H show in situ photoluminescence (PL) maps superimposed on the optical images of the thin films at Stages I–IV. The starting NH_4PbI_3 thin film appears non-luminescent with microscopic defects (Figure 2E, Stage I). After 1 s exposure to CH_3NH_2 gas, spots of PL appear (Figure 2F, Stage II). After 2 s, the PL signal vanishes completely (Figure 2G, Stage III), and the defects, as seen in Stages I and II, disappear as well. Finally, when the CH_3NH_2 gas is removed, PL signal is recovered rapidly (Figure 2H, Stage IV) within 2 s. Compared with Stage II, the PL map at Stage IV is obviously more uniform.

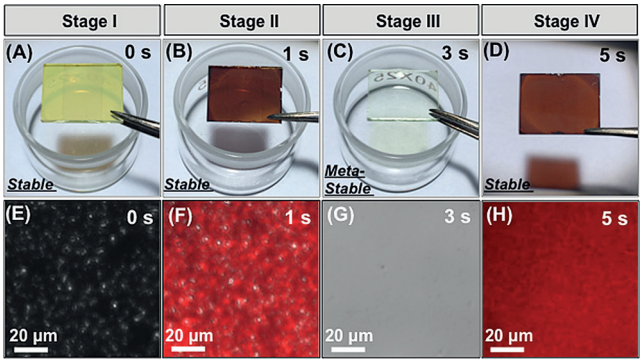

Figure 2. A–D) Photographs and E–H) photoluminescence maps (superimposed on optical microscope images) of the thin film at the four different stages described in Table 1.

The thin films at all stages were further studied using ex situ UV/vis spectroscopy and X-ray diffraction (XRD). Note that since the colorless film at Stage III is only stable under CH_3NH_2 gas, its UV/vis spectrum and XRD pattern (Figure S3 in the SI) were acquired using special enclosures containing CH_3NH_2 gas. The phase purity of the starting NH_4PbI_3 thin film (Stage I) is confirmed by the absorption edge at 520 nm in Figure 3A, and the XRD pattern in Figure 3B. The experimental and simulated XRD patterns of NH_4PbI_3 thin film are fully consistent (Figure S4 in the SI). At

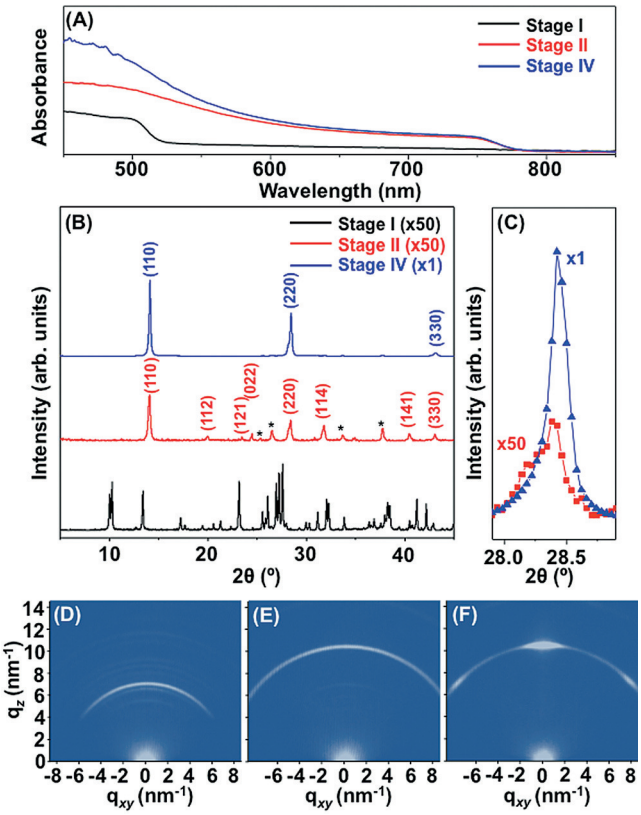

Figure 3. A) UV/vis spectra of Stage I, II and IV thin films, and B) corresponding XRD patterns (Stage II and IV thin film XRD intensities multiplied by 50). C) Comparison of the XRD intensities of the (220) diffraction peaks for Stage II and IV thin films. Corresponding 2D XRD patterns of thin films: D) Stage I, E) Stage II, and F) Stage IV.

Stage II, the light absorption increases significantly at all wavelengths, and the absorption edge extends to 776 nm, as seen in Figure 3A. This is in agreement with the observed darkening in Figures 1B and 2B. XRD pattern in Figure 3B confirms that only pure $MAPbI_3$ exists at this stage. At Stage III (Figure S3 in the SI), the thin film shows little absorption, and the corresponding XRD pattern is featureless. But at Stage IV, the absorption features of $MAPbI_3$ again evolve with an overall enhancement in the absorbance (Figure 3A). The corresponding XRD pattern in Figure 3B confirms the pure $MAPbI_3$ phase.[8] Interestingly, the XRD intensity of $MAPbI_3$ at Stage IV is several orders of magnitude higher than that at Stage I (Figure 3C). 2D XRD images of the thin film show typical random polycrystalline nature in Stage I and II films (Figures 3D and E), but strong 110 texture is observed in Stage IV film (Figure 3F).

The morphologies of the films at Stages I, II, and IV are characterized using ex situ scanning electron microscopy (SEM) and transmission electron microscopy (TEM). (Stage III thin film could not be characterized using SEM or TEM as it is only stable under CH_3NH_2 gas.) As seen in Figures 4A and D, the starting NH_4PbI_3 thin film (Stage I) appears porous, with a rough surface. At Stage II, the morphology of $MAPbI_3$ thin film (Figures 4B and E) essentially mirrors that of the starting NH_4PbI_3 thin film. However, at Stage IV

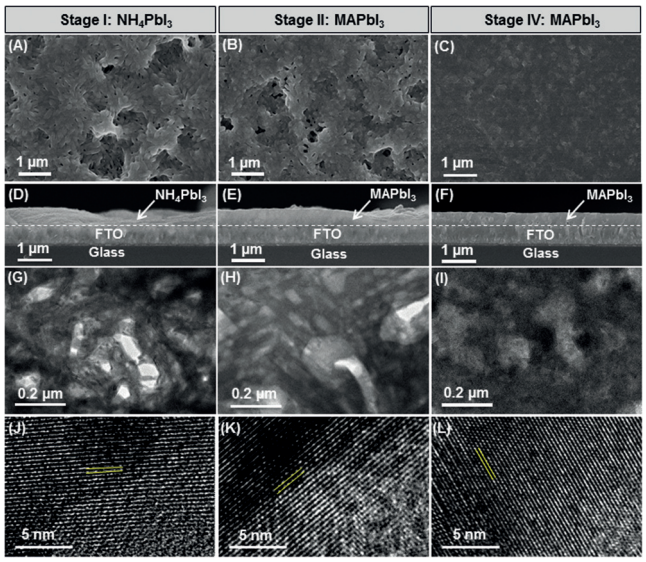

Figure 4. SEM images of thin films: A, D) Stage I, B, E) Stage II, and C, F) Stage IV. Corresponding TEM and HRTEM images: G, J) Stage I, H, K) Stage II, and I, L) Stage IV.

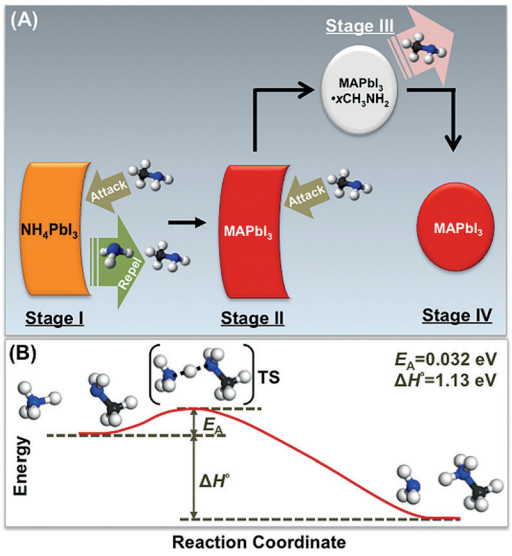

Figure 5. A) Proposed mechanism of the thin-film transformation of NH_4PbI_3 to $CH_3NH_3PbI_3$ via the methylamine-induced conversion–healing process. B) Plot of E_A and $\Delta H°$, calculated using DFT, as a function of reaction coordinate (not to scale).

(Figures 4C and F), the $MAPbI_3$ thin film becomes very smooth with a dense grain structure and uniform thickness. This change in morphology is in good agreement with in situ PL results. The porous structure of the sample at Stages I and II is clearly revealed by the contrast in the TEM images in Figures 4G and H, respectively, whereas the dense structure of the sample at Stage IV is confirmed in Figure 4I. The high-resolution TEM (HRTEM) images in Figures 4J–L show lattice fringes with interplanar spacing of 0.34 nm, 0.32 nm, and 0.32 nm, respectively, which can be indexed as (211) planes in NH_4PbI_3, and (220) planes in $MAPbI_3$.[6,8]

Based on the above characterization results of the NH_3PbI_4-to-$MAPbI_3$ transformation at various length scales, the mechanism of this process is proposed in Figure 5A. When NH_4PbI_3 non-perovskite is placed in the CH_3NH_2 gas atmosphere, a cation displacement reaction (Reaction 1) occurs that converts NH_4PbI_3 to $MAPbI_3$. Similar to the reaction of $MAPbI_3 + FA \rightarrow FAPbI_3 + MA$ in an earlier study,[9a] this NH_4PbI_3-to-$MAPbI_3$ conversion is morphology-preserving. That is, all the crystallographic characteristics in NH_4PbI_3 can be replicated in the as-converted $MAPbI_3$ after Reaction (1). In the subsequent step, a reversible reaction (Reaction (2)) occurs with the formation of an intermediate liquid $MAPbI_3{\cdot}x\,CH_3NH_2$, which is the result of the interaction between CH_3NH_2 and $MAPbI_3$.[9b] Owing to the liquid state of the intermediate phase, the crystal surfaces are readily smoothened after Reaction (2). In the thin film case, the solution-crystallized starting NH_4PbI_3 thin film is porous, rough, and polycrystalline (Stage I). After Reaction 1, the NH_4PbI_3 is converted to $MAPbI_3$, but the overall thin-film morphology is retained (Stage II). Upon further exposure to CH_3NH_2 gas, excess CH_3NH_2 is uptaken by $MAPbI_3$, resulting in the "melting" of the porous, rough perovskite thin film into the dense, smooth $MAPbI_3{\cdot}x\,CH_3NH_2$ liquid film (Stage III). After removal of the film from CH_3NH_2 gas, a dense, smooth and textured $MAPbI_3$ thin film (Stage IV) recrystallizes due to a self-degassing process.[9b]

$$NH_4PbI_3 + CH_3NH_2 \rightarrow CH_3NH_3PbI_3 + NH_3 \quad (1)$$

$$CH_3NH_3PbI_3 + x\,CH_3NH_2 \rightarrow CH_3NH_3PbI_3 \cdot x\,CH_3NH_2 \rightarrow CH_3NH_3PbI_3 + x\,CH_3NH_2 \quad (2)$$

The NH_4PbI_3-to-$MAPbI_3$ transformation process is reminiscent of the process involved in the $HPbI_3$–CH_3NH_2 interaction.[9c] However, there is an obvious difference between the two processes. In the case of $HPbI_3$, when CH_3NH_2 gas is introduced, the $HPbI_3$ crystal directly "melts" into the $MAPbI_3{\cdot}x\,CH_3NH_2$ liquid, and morphology-preserving conversion of $HPbI_3$ to $MAPbI_3$ is not observed. In the case of NH_4PbI_3, Reaction (1) not only forms $MAPbI_3$ product, but also generates NH_3 gas as a by-product. The release of NH_3 (vapor pressure 857 kPa at RT) from the solid grains resists the instantaneous ingression of CH_3NH_2 (vapor pressure 186.1 kPa at RT) into the as-nucleated $MAPbI_3$. In contrast, in the case of the reaction $HPbI_3 + CH_3NH_2 \rightarrow MAPbI_3$, there are no associated by-products, where the excess CH_3NH_2 is uptaken as soon as the perovskite nuclei form. In this situation, external heat is required to resist the excess-CH_3NH_2 ingression in order to enable the morphology-preserving $HPbI_3$-to-$MAPbI_3$ conversion.[9c] This is consistent with the fact that the NH_3 gas by-product has a similar effect. In another related study by Raga et al.,[9e] it appears that, in the presence of moisture or polar solvent vapor, a PbI_2 thin film first converts to $MAPbI_3$ perovskite in CH_3NH_2 atmosphere before the formation of $MAPbI_3{\cdot}x\,CH_3NH_2$. The perovskite formation reaction is described in that study as: $3\,PbI_2 + 2\,CH_3NH_2 + H_2O \rightarrow 2\,CH_3NH_3PbI_3 + PbO$, where the PbO by-product could also resist the CH_3NH_2 ingression. This further supports our proposed mechanism. Note that the

exact mechanisms are expected to be further revealed using higher-resolution in situ characterization techniques, which is the subject of a future study.

The facile nature of Reaction (1) is further confirmed by DFT calculations (see the SI for details). As shown in Figure 5, the activation energy (E_A) is as low as 32 meV for the chemical conversion of $NH_4^+ + CH_3NH_2 \rightarrow NH_3 + CH_3NH_3^+$ via a transition state of $H_3N{\cdot\cdot}H{\cdot\cdot}CH_2NH_2$. The enthalpy change ($\Delta H°$) involved in this chemical conversion is −1.13 eV. This suggests that the proton (H^+) transfer occurs readily when NH_4^+ and CH_3NH_2 contact each other, accelerating the cation switch. Considering that this chemical conversion occurs in a crystalline structure, the overall enthalpy change (ΔH) for Reaction (1) is further calculated to be −126 meV. These results confirm that Reaction (1) is highly favorable energetically, which explains the fact that the NH_4PbI_3 phase in the thin films coverts to $MAPbI_3$ in one second at RT. We investigated further the role of the compositions in the starting material on the transformation behavior, and explored the generality of such behavior to other $APbX_3$ compounds. As shown in Figure S5 in the SI, very similar behavior is observed with a starting NH_4PbBr_3 thin film, which indicates that the halogen anion does not have a significant impact on the overall chemical transformation process. This is expected considering that the chemical reaction involves A-site cations only. However, when the A site is occupied by an inorganic cation (e.g. Cs^+), the cation displacement reaction does not occur because of the absence of H^+ in the structure and the non-volatile nature of Cs (Figure S6 in the SI). As a result, only a less stable intercalation compound $CsPbI_3{\cdot}x\,CH_3NH_2$ forms after the $CsPbI_3$–CH_3NH_2 interaction, which converts back to $CsPbI_3$ upon mild heating. Similar interaction behavior between PbI_2 and pure CH_3NH_2 is also reported in the literature.[10] DFT results show that the bonding between CH_3NH_2 and $[PbX_6]$ is about an order of magnitude weaker than that between protonated CH_3NH_2 ($CH_3NH_3^+$) and $[PbX_6]$, which highlights the importance of H^+ being present in the starting materials for transformation into a stable perovskite structure. In the case of starting thin films with a long-chain alkylammonium lead iodide (e.g. $(C_{16}H_{33}NH_3)_2PbI_4$, which contains H^+ but with a much less volatile $C_{16}H_{33}NH_2$ component), transformation of $(C_{16}H_{33}NH_3)_2PbI_4$ to $MAPbI_3$ does not occur (Figure S7 in the SI). This can be attributed to the difficulty of complete displacement of the heavy $C_{16}H_{33}NH_3^+$ cation by MA^+, which suggests that the relative volatility of the A component is an important factor for the transformation behavior. In this context, the key to the success of the NH_4PbI_3-to-$MAPbI_3$ transformation is the fact that both criteria—presence of proton and A-site alkyl group volatility—are met simultaneously.

Finally, Stage I, II, and IV thin films are assembled into PSCs with TiO_2/FTO anodes and spiro-OMeTAD/Ag cathodes and their typical current density–voltage (J–V) curves are shown in Figure 6A. The PSC with the starting NH_4PbI_3 shows almost no PV response. After phase conversion to $MAPbI_3$ (Stage II), a power conversion efficiency (PCE) of 10.2% is reached, which is attributed to the intrinsic merits of $MAPbI_3$. The PCE is further increased to 15.4% with Stage IV film, which is in good agreement with the favorable structural characteristics of the final $MAPbI_3$ thin film (texture, uniformity, compactness) that are developed during the transformation process. The overall PV responses of the thin film during the transformation process are fully consistent with the evolution of the structural/physical properties at various length scales. (See complementary PV performance data in Figure S8 in the SI.) With further optimization in the processing and structure (Figure S9 in the SI), PSCs based on the transformed (Stage IV) thin films can deliver a PCE of 17.3% with suppressed hysteresis (Figure 6B), which demonstrates the promise of such thin film transformation behavior in PV application.

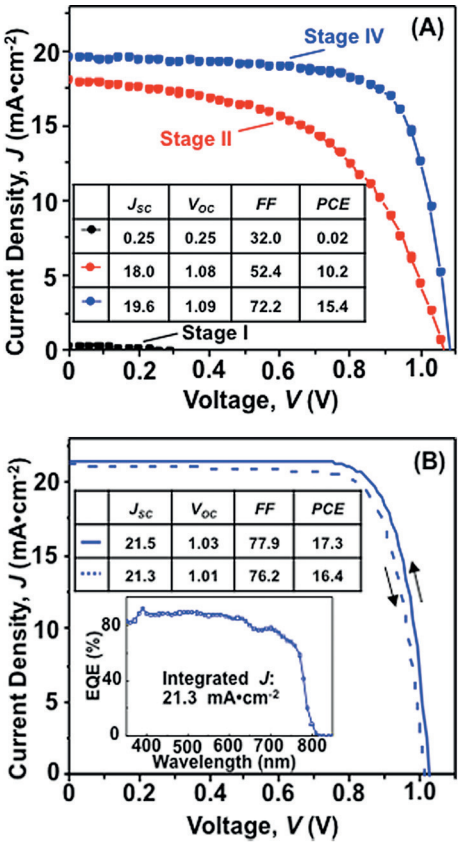

Figure 6. A) J–V responses of solar cells using Stage I, II, and IV thin films. B) J–V responses of the solar cell using the Stage IV thin film with optimal thickness, and the corresponding external quantum efficiency (EQE) spectrum (inset). The inset tables are extracted PV performance parameters. The units for J_{SC}, V_{OC}, FF, and PCE are $mA\,cm^{-2}$, V, %, and %, respectively.

In closing, the thin-film transformation of NH_4PbI_3 to $MAPbI_3$ has been studied for the first time, where two chemical sub-processes are involved. One is the morphology-preserving conversion of NH_4PbI_3 non-perovskite to $MAPbI_3$ perovskite via cation displacement. The other is a reversible transformation of solid–liquid–solid, which heals the structural defects in the as-converted $MAPbI_3$ thin film. Through this process a photo-inactive material (porous, rough, polycrystalline NH_4PbI_3 non-perovskite thin film) is converted stewise to an excellent PV material (dense, ultrasmooth, textured $MAPbI_3$). The discovery and mechanistic study of

such unusual chemical phenomenon demonstrate the existence of an unprecedented variety of phenomena and research opportunities in this fascinating class of hybrid materials, with implications for further understanding of the less-explored inorganic–organic hybrid chemistry.

Experimental Section

Materials and films synthesis: NH_4PbI_3 raw crystals were prepared using a room-temperature solvent-evaporation approach, as described in the SI. CH_3NH_2 gas was generated using a commercially purchased CH_3NH_2 (99%) gas tank or from a CH_3NH_2 ethanol solution (27–32 wt%). NH_4PbI_3 thin films were prepared by spin-coating a 45 wt% NH_4PbI_3 solution in DMF solution at 3000 rpm for 60 s, followed by thermal annealing at 100 °C for 10 min. Stage II, III, and IV films were fabricated by placing the starting (Stage I) NH_4PbI_3 films in CH_3NH_2 gas atmosphere for 1 s, 2 s, and 3 s, respectively.

Materials and films characterization: XRD patterns were obtained using an X-ray diffractometer (D8 Advance, Bruker, Germany) using Cu K_α radiation. UV/vis absorption spectra were recorded using a spectrometer (U-4100, Hitachi, Japan). A SEM (S-4800, Hitachi, Japan) and a TEM (2100F, JEOL, Japan) were used to characterize the morphology of the thin films. In situ PL mapping was conducted using a confocal laser scanning microscope (Fluo View FV1000, Olympus, Japan). In situ optical microscopy observations were carried out using a stereomicroscope (SZX16, Olympus, Japan). Further details are included in the SI.

Solar cell fabrication and testing: A 30-nm compact TiO_2 was deposited on the pre-patterned FTO-coated glass, followed by deposition of a 250-nm mesoporous TiO_2 layer. Then, the NH_4PbI_3 and/or $MAPbI_3$ perovskite layer were deposited using the procedures described above. The spiro-OMeTAD/Ag cathode was then deposited to complete the solar cell. *J–V* characteristics of the as-fabricated solar cells were measured under 1-sun illumination (Oriel Sol3A Class AAA, Newport, USA). Typical active area of the PSCs is 0.09 cm^2, as defined by a non-reflective metal mask. Further details are included in the SI.

Acknowledgements

Funding for this research from the International S&T Cooperation Program of China (2015DFG62670), Youth Innovation Promotion Association of CAS (2015167), and the U.S. National Science Foundation (DMR-1305913 and OIA-1538893) is gratefully acknowledged.

Keywords: hybrid perovskites · solar cells · thin films

How to cite: *Angew. Chem. Int. Ed.* **2016**, *55*, 14723–14727
Angew. Chem. **2016**, *128*, 14943–14947

[1] D. B. Mitzi in *Progress in Inorganic Chemistry, Vol. 48* (Ed.: K. D. Karlin), Wiley, New York, **1999**, pp. 1–122.
[2] a) W. Zhang, G. E. Eperon, H. J. Snaith, *Nat. Energy* **2016**, DOI: 10.1038/nenergy.2016.48; b) M. Grätzel, *Nat. Mater.* **2014**, *13*, 838–842; c) Y. Zhou, K. Zhu, *ACS Energy Lett.* **2016**, *1*, 64–67.
[3] a) A. Kojima, K. Teshima, Y. Shirai, T. Miyasaka, *J. Am. Chem. Soc.* **2009**, *131*, 6050–6051; b) H.-S. Kim, C.-R. Lee, J.-H. Im, K.-B. Lee, T. Moehl, A. Marchioro, S.-J. Moon, R. Humphrey-Baker, J.-H. Yum, J. E. Moser, M. Grätzel, N.-G. Park, *Sci. Rep.* **2012**, *2*, 591.
[4] a) C. C. Stoumpos, M. G. Kanatzidis, *Acc. Chem. Res.* **2015**, *48*, 2791–2802; b) Y. Zhou, O. S. Game, S. Pang, N. P. Padture, *J. Phys. Chem. Lett.* **2015**, *6*, 4827–4839; c) Y. Zhao, K. Zhu, *Chem. Commun.* **2014**, *50*, 1605–1607; d) T. Zhang, N. Guo, G. Li, X. Qian, Y. Zhao, *J. Mater. Chem. A* **2016**, *4*, 3245–3248; e) S. R. Raga, L. K. Ono, Y. Qi, *J. Mater. Chem. A* **2016**, *4*, 2494–2500.
[5] G. Kieslich, S. Sun, A. K. Cheetham, *Chem. Sci.* **2015**, *6*, 3430–3433.
[6] L.-Q. Fan, J.-H. Wu, *Acta Crystallogr. Sect. E* **2007**, *63*, i189.
[7] M. Green, *Third Generation Photovoltaics*, Springer, Berlin, **2003**.
[8] a) Y. Zhou, M. Yang, W. Wu, A. L. Vasiliev, K. Zhu, N. P. Padture, *J. Mater. Chem. A* **2015**, *3*, 8178–8184; b) Y. Zhou, A. L. Vasiliev, W. Wu, M. Yang, S. Pang, K. Zhu, N. P. Padture, *J. Phys. Chem. Lett.* **2015**, *6*, 2292–2297.
[9] a) Y. Zhou, M. Yang, S. Pang, K. Zhu, N. P. Padture, *J. Am. Chem. Soc.* **2016**, *138*, 5535–5538; b) Z. Zhou, Z. Wang, Y. Zhou, S. Pang, D. Wang, H. Xu, Z. Liu, N. P. Padture, G. Cui, *Angew. Chem. Int. Ed.* **2015**, *54*, 9705–9709; *Angew. Chem.* **2015**, *127*, 9841–9845; c) S. Pang, Y. Zhou, Z. Wang, M. Yang, A. Krause, Z. Zhou, K. Zhu, N. P. Padture, G. Cui, *J. Am. Chem. Soc.* **2016**, *138*, 750–753.
[10] R. F. Warren, W. Y. Liang, *J. Phys. Condens. Matter* **1993**, *5*, 6407–6418.

Received: September 28, 2016
Published online: October 21, 2016

